Microporous and Mesoporous Materials 135 (2010) 2–8

Contents lists available at ScienceDirect

Microporous and Mesoporous Materials

journal homepage: www.elsevier.com/locate/micromeso

Physico-chemical characterization of nitrided mesoporous silicon MCM-41

Guangjun Wu [a], Shaoliang Jiang [a], Landong Li [a], Fuxiang Zhang [a], Yali Yang [a], Naijia Guan [a,*], Mihail Mihaylov [b,c,1], Helmut Knözinger [b,**]

[a] Key Laboratory of Functional Polymer Materials (Nankai University), Ministry of Education, Tianjin 300071, People's Republic of China
[b] Department Chemie und Biochemie, LMU München, Butenandtstrasse 5 – 13, D-81377 München, Germany
[c] Institute of General and Inorganic Chemistry, Bulgarian Academy of Sciences, Acad. G. Bonchev Str., Bld. 11, Sofia 1113, Bulgaria

ARTICLE INFO

Article history:
Received 8 May 2009
Received in revised form 26 May 2010
Accepted 2 June 2010
Available online 8 June 2010

Keywords:
Nitridation
MCM-41
N species
IR spectroscopy
Base catalysis

ABSTRACT

Mesoporous nitrided MCM-41 was synthesized and physically characterized. The nitrogen species are predominantly present as imido NH groups as shown by infrared spectroscopy. The NH groups are located in the framework and are therefore inaccessible for reactant and probe molecules. Deuterium exchange experiments support this interpretation. The surface exposes Si–OH groups which are identical to silanol groups on pure silica; basic sites could not be detected by neither deutero-chloroform nor methylacetylene. We infer that a small number of NH_2 groups are located at the surface of the pore walls which may be responsible for the activity for base-catalyzed reactions.

1. Introduction

Solid basic materials have attracted increasing interest in the recent past, since they are environmentally friendly and have shown potential as catalysts for a number of industrially important reactions, especially for fine chemical synthesis [1]. Porous materials, such as mesoporous silica and microporous zeolites, are families of solids having unique structures and morphologies, and high surface areas, and they can serve as parent porous materials for the production of solid base catalysts. Conventionally, solid basic porous materials are obtained via ion exchange with alkali metal cations [2–4], incorporation of alkaline earth metal oxides [3,4], impregnation with alkali metal ions/basic salts [5,6], deposition of basic guests in the cavities [7], isomorphous substitution of silicon by germanium in the framework [8], and grafting of organic functional moieties onto the pore walls [9–11]. However, these materials suffer from several shortcomings such as low strength of basic sites, partial blockage of the pores, and sensitivity of the basic guests towards CO_2 or moisture in the air [12].

Nitridation at elevated temperature is a completely different approach to synthesize solid basic materials, by which framework O atoms are partially substituted by NH_x groups. Compared with conventionally prepared materials, nitrided oxidic materials possess several advantages. They exhibit properties of preceramic intermediates and as such have only low sintering tendency, so that high specific surface areas are retained even after severe thermal treatments [13]. In addition, they are structurally stable at elevated temperatures [12,13]. Till now, nitrogen-incorporated amorphous aluminum orthophosphate [14–16], various mesoporous silicas (such as FSM-16 [17], MCM-48 [18], SBA-15 [19,20], MCM-41 [21,22]), mesoporous silica thin films [23–25], and microporous zeolites (such as NaY [26,27], AlPO-5 [28], SAPO-11 [29], ZSM-5 [30,31], SAPO-34 [32], Beta [33], and B-SSZ-13 [34]) have been synthesized by high-temperature ammonia treatment and tested after nitridation as basic porous materials. The nitrogen content can be controlled by the temperature treatment and determines the basicity of the nitrogen-containing materials [34,35]. Compared with microporous zeolites, the maximum nitrogen content of mesoporous silica is higher and can reach values as high as 25 wt.%, which corresponds to >60% of O atoms being substituted by N atoms [21]. However, even though most of the nitrided materials have shown good activity for the Knoevenagel condensation, a typical test reaction for the performance of basic solids [15], the density of basic sites and the base strength do still not satisfy the requirements for industrial application. Also, the chemical nature of the basic sites generated by nitridation remains to be clarified [12].

In the present paper, nitrogen-containing MCM-41 zeolites with high nitrogen content were synthesized by nitridation in an ammonia flow at elevated temperatures. The influence of the

* Corresponding author. Tel./fax: +86 22 2350 0341.
** Corresponding author. Tel./fax: +49 89 2180 77604/77605.
E-mail addresses: guannj@nankai.edu.cn (N. Guan), helmut.knoezinger@cup.uni-muenchen.de (H. Knözinger).
[1] Tel.: +359 2 9792556; fax: +359 2 705024.

1387-1811/$ - see front matter © 2010 Elsevier Inc. All rights reserved.
doi:10.1016/j.micromeso.2010.06.003

nitridation on the physico-chemical properties of the nitrogen-containing mesoporous materials were investigated by XRD, N_2 adsorption, and ^{29}Si-MAS-NMR for reasons of comparability with previously published investigations. To the best of our knowledge, an in depth characterization of the acido-basic surface properties of this class of mesoporous materials has not been reported so far. Therefore, we describe here experimental attempts to fill this gap by means of infrared spectroscopy of adsorbed probe molecules.

2. Experimental

2.1. Preparation of nitrided MCM-41

The parent MCM-41 mesoporous molecular sieve was prepared via hydrothermal synthesis as reported by Liu et al. [36] and calcined at 550 °C to remove the template. Nitridation of the parent MCM-41 was carried out in the temperature range of 600–1000 °C in a quartz tube at constant NH_3 flow (400 $cm^3\ min^{-1}$) for 12 h. Ammonia (99%) and dinitrogen (99.999%) were delivered by Tianjin Liufang Gas Company.

These conditions were chosen because the saturation N content was reached. Subsequently the samples were slowly cooled down to room temperature under flowing N_2 and stored under dry N_2. The nitrided samples are denoted MCM-41-600N, MCM-41-700N, MCM-41-800N, MCM-41-900N, and MCM-41-950N, indicating that the as-synthesized material was treated in the NH_3 flow at 600, 700, 800, 900, and 950 °C, respectively.

2.2. Characterization

Nitrogen contents were examined by alkaline digestion with molten NaOH at 400 °C. The evolving NH_3 was absorbed in H_2SO_4 solution (0.15 mol L^{-1}) which was then titrated by NaOH solution (0.15 mol L^{-1}). The detailed description of the procedure can be found in the literature [37].

Powder X-ray diffraction (XRD) patterns were measured on a D/Max-2500 powder diffractometer (operated at 36 kV and 20 mA) using Cu K_α (λ = 1.54178 Å) radiation from 1° to 10° with a scan speed of 2θ = 4.0 deg min^{-1}.

Nitrogen adsorption/desorption measurements were performed at liquid N_2 temperature using a NOVA 1000e apparatus (Quantachrome Co.) after outgassing the samples for 2 h at 300 °C under vacuum. Surface areas were calculated according to the conventional BET method. The adsorption branches of the isotherms were used for the calculation of the pore parameters using the BJH method.

Solid-state ^{29}Si NMR measurements at room temperature were performed on a Varian Infinity Plus-400 spectrometer equipped with a 4 mm probe (MAS was set to 6 kHz). The instrument was operated at 79.4 MHz and the 90° pulse sequence was 3 μs.

IR spectra of the samples were recorded in transmission prior to and after adsorption of probe molecules on a Bruker IFS-66 spectrometer at a spectral resolution of 2 cm^{-1}; each spectrum was the average of 128 scans. The IR cell was purpose-made for recording spectra *in situ* at temperatures between −185 °C and ambient temperature. The cell was connected to a vacuum adsorption system with a base pressure below 10^{-3} Pa. Self-supporting wafers of the samples were thermoevacuated in the cell at 490 °C for 1 h to remove contaminations and adsorbed water. After recording the background spectra, the adsorption of various probe molecules was detected by their vibrational spectra in the adsorbed state. The probe molecules included carbon monoxide CO (99. 997% purity from Linde AG), trichloro methane-d_1 $CDCl_3$ (99.8 atom% D from Merck AG), methyl acetylene H_3CCCH (98%, from Lancaster Synthesis). Deuterium exchange of OH and NH_x groups in the solid materials and/or at their surfaces was tested using D_2 (99.7% from Messer Griesheim GmbH) and deuterium oxide D_2O (99.9% D from Cambridge Isotope Laboratories, Inc.) at temperatures 200–490 °C.

2.3. Catalytic evaluation

The basic catalytic properties of nitridation samples were evaluated by Knoevenagel condensation. Benzaldehyde (25 mmol), malononitrile (25 mmol) and 40 ml of toluene (chemicals (AR) were delivered by Tianjin KRS Fine Chemical Co. Ltd.) were added into a round bottom flask (volume 100 ml) which was equipped with a magnetic stirrer and a reflux condenser and immersed in a thermostatic oil bath. Once the mixture reached 323 K, 0.4 g catalyst was added into the flask. Small liquid samples of 0.5 μl were then periodically withdrawn from the reaction mixture with a syringe and analyzed in a SP-502 gas chromatograph equipped with a FID and a 0.2 mm × 50 m FFAP capillary column.

3. Results and discussion

3.1. Physico-chemical properties of nitrided MCM-41

The N-content of nitrided MCM-41 was determined by a wet analytical method as described in Section 2.1. The data are summarized in Table 1. They clearly show that the incorporation of nitrogen atoms by substitution of oxygen atoms requires elevated temperatures preferably beyond 800 °C. The higher the nitridation temperature, the higher is the ultimate N-content after 12 h nitridation with 26.0 wt.% being the highest N-content yielded in sample MCM-41-950N. The incorporation of nitrogen atoms into the MCM-41 matrix is also supported by ^{29}Si-MAS-NMR and infrared spectra (see Section 3.2 below).

The pore structure and surface areas were determined by N_2 adsorption measurements at −196 °C. The isotherms of the parent MCM-41 and of the nitrided variants are shown in Fig. 1. All as-synthesized samples exhibit type IV isotherms with a typical capillary condensation step with virtually no hysteresis suggesting the presence of almost uniform pores. The relative pressure of the capillary condensation step for the parent MCM-41 is 0.35–0.43. After nitridation, the relative pressures of the capillary condensation step for the MCM-41-600N, MCM-41-800N, MCM-41-900N, and MCM-41-950N shift to 0.20–0.35, 0.18–0.26, 0.18–0.26, and 0.15–0.26 respectively. Obviously, the relative pressure of capillary condensation gradually decreases with the increase of nitridation temperature. The average pore radius of the nitrogen-free parent MCM-41 was first increases from 2.7 nm to 2.92 nm after thermal treatment in ammonia and then decreases to 2.24 nm after treatment in an ammonia flow at 950 °C.

Specific surface areas are also shown in Table 1. The parent MCM-41 material has the highest specific surface area of 1150 $m^2\ g^{-1}$, which decreases for nitrided samples as the nitridation temperature increases. The specific surface areas of MCM-

Table 1
N content, average pore radii, pore volumes and specific surface areas of nitrided MCM-41.

Sample	N content (wt.%)	Average pore radius (nm)	Pore volumes ($cm^3\ g^{-1}$)	Specific surface areas ($m^2\ g^{-1}$)
MCM-41	–	2.70	1.4891	1150
MCM-41-600N	3.0	2.92	0.4864	1102
MCM-41-800N	10.9	2.88	0.3483	1007
MCM-41-900N	19.4	2.64	0.2596	996
MCM-41-950N	26.0	2.24	0.579	960

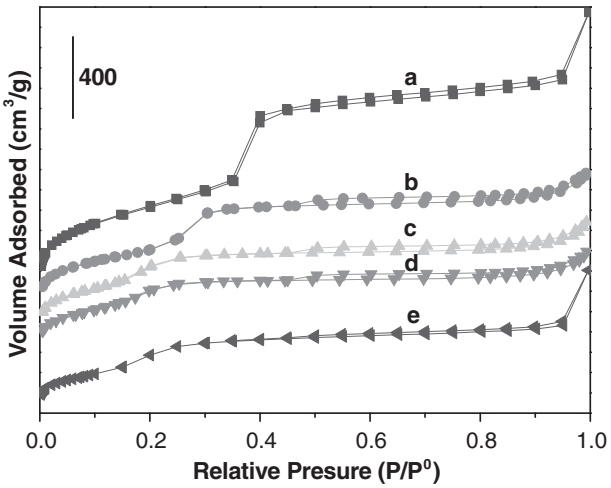

Fig. 1. Nitrogen sorption isotherms of MCM-41 (a), MCM-41-600N (b), MCM-41-800N (c), MCM-41-900N (d) and MCM-41-950N (e).

41-600N, MCM-41-800N, MCM-41-900N, and MCM-41-950N are lower by 4%, 12%, 13%, and 17%, respectively, relative to the parent material. Nevertheless, sample MCM-41-950N has still a high surface area of 960 $m^2\ g^{-1}$, suggesting that the nitrided samples maintain a largely unchanged morphology as compared with the parent material when the nitridation temperature is not higher than 950 °C. This will be further discussed on the basis of XRD diffraction data (Fig. 2).

The structural and morphological order of nitrided samples was investigated by X-ray diffraction. Fig. 2 shows the XRD patterns of MCM-41 before and after nitridation at temperatures of 800, 900, 950, and 1000 °C. The XRD pattern for the parent MCM-41 is typical for a highly ordered hexagonal mesophase material. Qualitatively, the XRD patterns are also consistent with these structural characteristics for samples that had been nitrided at temperatures not higher than 950 °C. Compared to parent MCM-41, the intensities of the (1 0 0) peak of nitrided samples gradually decrease with increasing nitridation temperature. However, the sample nitrided at 950 °C still possessed a highly ordered hexagonal mesophase and large surface area. Besides the high thermal and hydrothermal stability of MCM-41, it was suggested that the ammonia atmosphere is a very important fact in maintaining structural ordering during nitridation [21,33]. After nitridation at 1000 °C, the (1 0 0) peak intensity is extremely low suggesting the breakdown of the mesophase structure at this temperature.

The (1 0 0) peak shifts to higher 2θ values as the nitridation temperature is increased in the 800–950 °C temperature range. This suggests shrinkage of the unit cell dimensions, which may be related with the decrease of the specific surface areas with increasing nitridation temperature (see Table 1).

The contraction of the unit cell is also documented by the shift of 2θ to greater values of the (1 1 0) and (2 0 0) peaks with increasing N content. Simultaneously, the intensities of these diffraction peaks decreases, which might be caused by a loss of long range order.

3.2. Characterization of N species in the framework

^{29}Si-MAS-NMR is a useful technique for the determination of the chemical environment of Si atoms in nitrogen-containing microporous and mesoporous zeolites. As shown in Fig. 3, the parent MCM-41 zeolite exhibits a dominating peak at −109 ppm, a shoulder at −99 to −105 ppm and a little peak at −90 ppm.

These peaks are assigned to $Si*(OSi)_4$, $HOSi*(OSi)_3$ and $(HO)_2Si*(OSi)_2$, respectively [35,38,39]. After nitridation, four new peaks are progressively growing in at −90, −75, −63, and −48 ppm at the expense of the original signals. These peaks are ascribed to $SiNO_3$, SiN_2O_2, SiN_3O, and SiN_4, respectively, according to the relevant literature on silicon oxynitrides [40] and nitrogen-containing mesoporous silica [20]. When the sample was nitrided at 600 °C, the dominating peak was split into two peaks (one is at −115 ppm assigned to $Si*(OSi)_4$ and another is at −105 ppm assigned to $HOSi*(OSi)_3$), indicating the formation of $HOSi*(OSi)_3$ groups at significant abundance by nitridation. When the nitridation temperature is raised to 800 °C, the peak assigned to

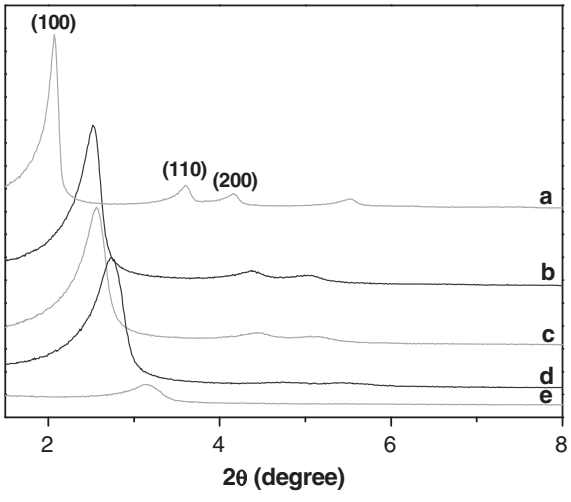

Fig. 2. XRD patterns of parent MCM-41 and of MCM-41 nitrided at different temperatures: untreated MCM-41 (a), MCM-41-800N (b), MCM-41-900N (c), MCM-41-950N (d) and MCM-41-1000N (e).

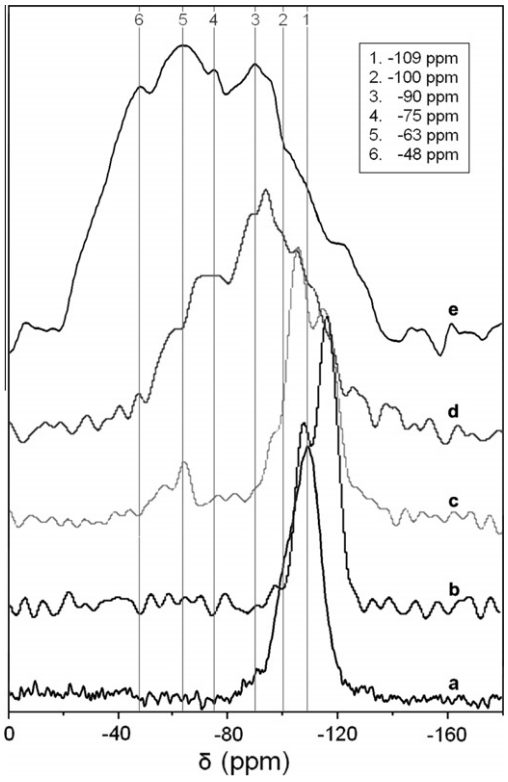

Fig. 3. ^{29}Si MAS-NMR spectra of MCM-41 (a), MCM-41-600N (b), MCM-41-800N (c), MCM-41-900N (d) and MCM-41-950N (e).

$HOSi*(OSi)_3$ groups becomes dominating. Meanwhile, a new peak at -63 ppm ascribed to SiN_3O is observed. In the spectrum of MCM-41-900N, the intensities of peaks assigned to $Si*(OSi)_4$ and $HOSi*(OSi)_3$ decrease and the peaks assigned to $SiNO_3$, SiN_2O_2, SiN_3O became more obvious. When the temperature was further increased to 950 °C, the peaks of $Si*(OSi)_4$ and $HOSi*(OSi)_3$ almost disappear and the SiN_4 phase was formed. Undoubtedly, the peaks attributed to $SiNO_3$, SiN_2O_2, SiN_3O, and SiN_4 are dominating in the spectrum of MCM-41-950N. This unambiguously confirms that the N atoms have been incorporated into the framework of MCM-41 by nitridation.

The infrared spectrum of the parent MCM-41 at frequencies below 1500 cm^{-1} is characterized by lattice vibrations with an intense antisymmetric Si–O–Si stretching band at 1100 cm^{-1} and a weaker symmetric stretching band at 812 cm^{-1} (not shown). On nitridation at 950 °C the latter band is almost quantitatively eroded, while the antisymmetric stretching band is shifted to 960 cm^{-1} with a shoulder near 1100 cm^{-1}. This effect may be interpreted as originating from increasing disorder of the MCM-41 lattice and higher bond strain by the incorporation of N-atoms in the lattice.

The transmission infrared spectra of nitrided MCM-41 samples in the wavenumber range between 1300 and 4000 cm^{-1} are shown in Fig. 4. The background spectra in this frequency regime of samples prior to nitridation are identical to spectrum a in Fig. 4 of sample MCM-41-600N, the N content of which is too small for detection in the infrared spectrum. The samples were thermoevacuated *in situ* at 490 °C for 1 h prior to recording the spectra. The sharp bands at 3742 cm^{-1} in all four spectra are typical for unperturbed surface silanol groups, while the diffuse absorption towards lower wavenumbers indicates the presence of H-bonded surface and intraparticle hydroxyl groups. In the NH_x stretching region [41] one band at 3388 cm^{-1} grows in on nitridation and first appears after nitridation at 700 °C. The intensity of this band increases with increasing nitridation temperature in agreement with the increasing N-content in the samples (*vide supra*). A second very weak band at 1555 cm^{-1} becomes detectable for N-rich samples after nitridation at high temperatures (see e.g. spectrum d in Fig. 4).

Bands at similar positions have been observed for various oxynitride materials. Most publications that report infrared data concentrated on the frequency region of lattice vibrations. The band assignments in the literature are not perfectly consistent. Climent et al. [16] investigated aluminophosphate oxynitrides and reported a band at 3480 cm^{-1} which they identified as the antisymmetric NH_2 stretching mode of Me–NH_2 groups (Me = Al or P), while a second band at 3370 cm^{-1} was attributed to the symmetric NH_2 stretching band and mainly the N–H stretching band of Me–NH–Me groups. A band at 1550 cm^{-1} was assigned to the symmetric deformation mode of terminal NH_2 groups consistent with the observation of the corresponding antisymmetric and symmetric stretching bands. Adsorbed ammonium ions and ammonia molecules were also reported. Analogous vibrational spectra were reported by Fripiat et al. [42] for nitrogenous species in zirconium phosphate oxynitrides and by Wang and Liu [20] in nitrided SBA-15. Busca et al. [43] investigated largely amorphous silicon nitride prepared by nitridation of amorphous silica with ammonia at elevated temperatures. Bands at 3370 and 1550 cm^{-1} were observed and assigned to N–H stretching and deformation bands of Si_2NH groups, respectively. In contrast, Kaskel and Schlichte [44] reported bands at 1548 and 1180 cm^{-1} in porous silicon nitride which they assigned to the deformation modes of amido NH_2 and imido NH groups, respectively.

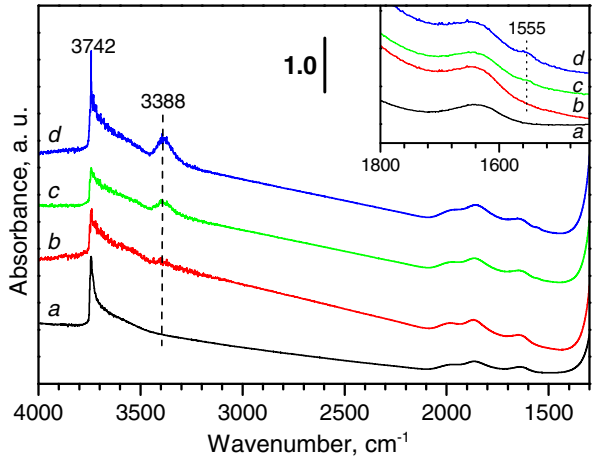

Fig. 4. IR spectra of N-containing MCM-41 silicas *in situ* thermoevacuated at 490 °C for 1 h: MCM-41-600N (a), MCM-41-700N (b), MCM-41-800N (c) and MCM-41-900N (d). Inset shows expanded region 1800–1450 cm^{-1}.

In our spectra of the nitrided MCM-41, only one band is seen at 3388 cm^{-1} in the N–H stretching region. We infer that this is good evidence for the presence of predominantly Si_2NH groups in the nitrided MCM-41, since amido groups would give rise to a doublet of the antisymmetric and symmetric N–H stretching modes. However, the very weak band at 1555 cm^{-1} might be assigned to the deformation mode of Si–NH_2 groups and hence, indicate the formation of amido minority species at the highest nitridation temperatures. It is important to note that the band at 3388 cm^{-1} is relatively broad. We infer that this is most likely due to the incorporation of the NH species in the framework of the mesoporous solid rather than being an unperturbed surface group.

The detection of the two infrared bands at 3388 and 1555 cm^{-1} is an important observation since it is clear evidence for the stability of the Si_2NH and Si–NH_2 groups even during thermoevacuation at a temperature as high as 490 °C. The intensities of the imido stretching band increase with increasing nitridation temperature in full agreement with the results of the quantitative chemical analysis (see Section 3.1 and Table 1). It is also important to note that the intensity of the band at 1555 cm^{-1} is typically very low in comparison with that of the band at 3388 cm^{-1}. We conclude from these results that the imido NH and amido NH_2 groups are formed during thermal treatment in an ammonia atmosphere in the temperature range 600–950 °C and, most importantly, that they are thermally stable even at 490 °C in the absence of ammonia. The density of NH groups is clearly dominant while that of NH_2 groups is close to the detection limit. We infer that the NH groups are likely located in the framework of the pore walls. This conclusion will be discussed in more detail below.

Results of deuterium exchange experiments shown in Fig. 5 also emphasize the fact that the NH species are located in the framework. In these experiments a MCM-41-900N wafer was thermally activated *in situ* in the infrared cell at 490 °C for 1 h. The corresponding spectrum a is shown in Fig. 5. The silanol band at 3742 cm^{-1} and the N–H stretching band at 3388 cm^{-1} are clearly seen. The wafer was then exposed to a D_2 atmosphere (100 h Pa) at 200 °C for 1 h (spectrum b in Fig. 5) followed by an additional treatment at 300 °C and otherwise identical conditions (spectrum c in Fig. 5). At this point, the N–H stretching band at 3388 cm^{-1} still remained almost unaffected (no H–D exchange) whereas the intensity of the silanol band at 3741 cm^{-1} is reduced by more than 50% and a SiO–D band grows in at 2759 cm^{-1}. The ratio of the wavenumbers is 1.36 and corresponds to the expected isotope ratio in harmonic oscillator approximation. Thus H–D exchange has clearly occurred with the silanol groups but not with the NH species. We therefore conclude that the latter species are preferentially located in the framework of the pore walls of the MCM-41 as already in-

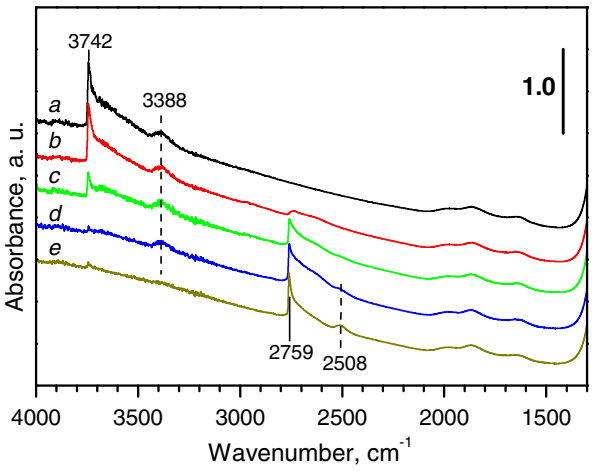

Fig. 5. IR spectra of MCM-41-900N: evacuated at 490 °C for 1 h (a), treated in D_2 (100 h Pa) at 200 °C for 1 h (b), treated in D_2 (100 h Pa) at 300 °C for 1 h (c), treated in D_2O (15 h Pa) at 300 °C for 1 h and evacuated at 300 °C for 15 min (d), treated in D_2O (20 h Pa) at 490 °C for 1 h and evacuated at 490 °C for 10 min (e).

ferred above. Although D_2 may well penetrate into the framework of the matrix, the molecule can most probably not be dissociated and is therefore not activated for H–D exchange.

In an additional experiment, the D_2 atmosphere was replaced by D_2O (15 h Pa) at 300 °C for 1 h and the cell was evacuated for 15 min (spectrum d in Fig. 5). H–D exchange with the NH species did occur under these conditions as shown by the appearance of a weak band at 2508 cm^{-1} and a decrease of the intensity of the N–H stretching band at 3388 cm^{-1} (spectrum d in Fig. 5) with a wavenumber ratio of 1.35. When in a final experiment the exchange was carried out in D_2O atmosphere at 490° C, the H–D exchange was quantitative with only OD and ND species being detectable. These experiments show, that heavy water undergoes H-bonding interactions with OH and NH groups thus forming H-bonded networks which allow proton mobility and exchange provided the temperature is high enough.

3.3. Acido-basic properties of nitrided MCM-41

Lewis acid sites are not expected to be present on the surface of MCM-41. The acido-basic properties of these materials and their nitrided forms should be determined by the presence of Si–OH groups, O atoms and NH groups in N-containing materials. The silanol groups may function as weakly acidic Bronsted (protonic) sites while the O atoms can act as Bronsted basic sites. These sites can be identified and characterized by their interaction with probe molecules, which is investigated by infrared spectroscopy [45–52]. Note that silanol groups are H-bond donors while oxygen atoms and eventually NH groups are H-bond acceptor sites. The H-bond interactions provide important information on the proton donor and acceptor properties of the respective surface sites when appropriate probe molecules are adsorbed on the oxide sample (Hydrogen Bonding Method). Interactions of a H-bond acceptor molecule with surface hydroxyl sites induce a red shift of the O–H stretching band which is a measure of the Bronsted acid strength [45–52]. Analogously, H-bond formation between a surface O atom and a H-bond donor probe molecule XH (e.g. CH acid molecule) results in a red shift and broadening of the X–H stretching band. The observed wavenumber shifts are a measure of the strength of the H-bond which is directly correlated with the donor strength (acid strength) or the acceptor strength (base strength) of silanol groups or oxygen atoms, respectively.

In Section 3.3.1, we describe the infrared spectroscopic results for the adsorption of carbon monoxide CO [52–54].

In Section 3.3.2, we analyze the infrared spectra of adsorbed CH acids, namely deuterochloroform $DCCl_3$ [55,56] and methylacetylene CH_3CCH [57] for the characterization of basic sites (oxygen atoms, NH_x groups).

3.3.1. Characterization of surface sites on nitrogen-containing MCM-41 by adsorption of carbon monoxide

Fig. 6 shows the infrared spectra of CO adsorbed on sample MCM-41-900N. The material was evacuated in *situ* at 490 °C prior to adsorption of CO. The background spectrum clearly shows the N–H stretching band at 3388 cm^{-1}. This band remains entirely unaffected by the exposure of the sample in CO although one might expect N–H. . .CO H-bonding interactions to occur at low temperatures. This observation is fully consistent with the inference that these groups are incorporated in the solid bulk matrix and therefore not accessible to the probe molecule.

The intensity of the characteristic silanol band at 3742 cm^{-1} in the background spectrum decreases dramatically on exposure to CO at −185 °C and simultaneously a shifted and broadened band at 3646 cm^{-1} grows in, clearly suggesting the formation of H-bonding interactions. The corresponding carbonyl vibration is observed at 2158 cm^{-1} in spectrum b of Fig. 6. The wavenumber shift of the hydroxyl stretching band of 96 cm^{-1} reproduces perfectly the shifts that are reported for low-temperature adsorption of CO on pure silica [58–60]. The carbonyl band position also coincides with those reported in the literature for CO adsorbed on silicas at low temperature [58,59]. The weak shoulder at 2140 cm^{-1} represents the presence of physically adsorbed CO. It should be noted that Hadjiivanov et al. [61] observed a carbonyl band at 2140 cm^{-1} when CO was adsorbed on titanium oxynitride at low temperatures. They assigned this band to CO interacting with O^{2-} anions.

Based on our present results, we conclude that there is no interaction detectable between the incorporated nitrogen-species and the CO probe; the MCM-41-900N shows the same properties as pure silica.

In conclusion, the infrared spectra of the adsorbed probe molecule CO consistently show that the only adsorption sites for this probe molecule on the nitrided MCM materials are silanol groups and that NH_x species are inaccessible for CO.

3.3.2. Search for basic sites by adsorption of CH-acids

Deuterochloroform $CDCl_3$ and methylacetylene CH_3CCH are CH-acids which are expected to form H-bonds with basic sites. Unfortunately, however, these molecules have H-bond acceptor proper-

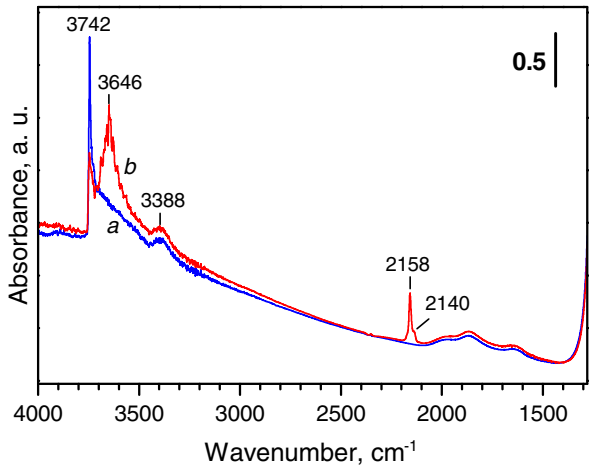

Fig. 6. IR spectra of MCM-41-900N evacuated at 490 °C for 1 h (a) and after adsorption of CO (125 Pa equilibrium pressure) at −185 °C (b).

ties in addition to their H-bond donor properties. Thus, $CDCl_3$ as a donor can form B...D–CCl_3 (B symbolizes a basic site) complexes and in addition as an H-bond acceptor it may undergo O–H...$ClCl_2CD$ interactions.

Fig. 7 shows the vibrational spectra of the chloroform probe molecule on MCM-41-600N and MCM-41-900N. Clearly, the N–H band at 3388 cm^{-1} remains unaffected, suggesting that basic sites are not available or not accessible on the surface of sample MCM-41-900N after *in situ* activation at 490 °C. In contrast, the silanol group interacts with chloroform. The position of the band is red-shifted by 57 cm^{-1}. For the adsorption of chloroform on amorphous silica a wavenumber shift of 48 cm^{-1} was reported [60].

Fig. 8 shows the infrared spectra of methylacetylene on MCM-41-600N and MCM-41-900N. The crucial normal modes of the gas phase C_3H_4 molecule are the C–H stretching mode at 3334 cm^{-1} and the C–C stretching band at 2138 cm^{-1} [51,56]. This probe molecule should be able to interact with basic surface sites via its C–H acid function with formation of a H-bond. This H-bond would be characterized by a red shift and broadening of the ν(C–H) vibration. The lack of these spectral changes suggests that basic sites are not present on the surface or cannot be reached by the probe molecule. The N–H band remains practically unchanged by the presence of the methylacetylene. Dramatic changes are seen in the OH stretching region where the intensity of the hydroxyl stretching band at 3742 cm^{-1} decreases and an intense and broadened band grows in at 3569 cm^{-1} characteristic for H-bonding. In the present case, the probe molecule forms a π-complex between the triple bond and the proton of the silanol group. The CH acid function of the probe molecule (C–H stretching band at 3294 cm^{-1}) is not directly involved in the adsorption interaction. In other words, methylacetylene also does not detect any basic sites.

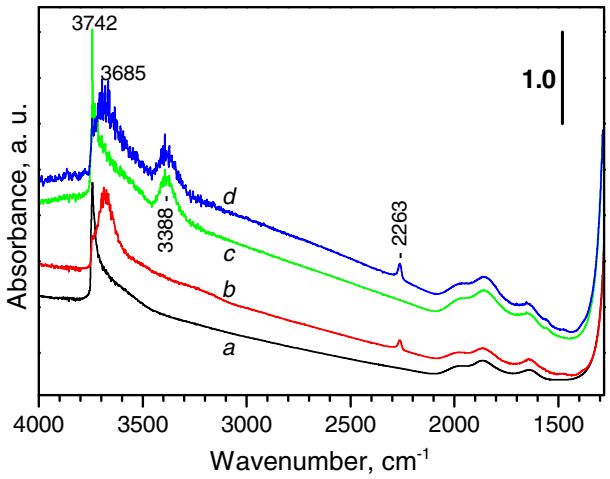

Fig. 7. IR spectrum of MCM-41-600N evacuated at 490 °C for 1 h (a) and after adsorption at r.t. of $CDCl_3$ (30 h Pa) (b). IR spectrum of MCM-41-900N evacuated at 490 °C for 1 h (c) and after adsorption at r.t. of $CDCl_3$ (30 h Pa) (d).

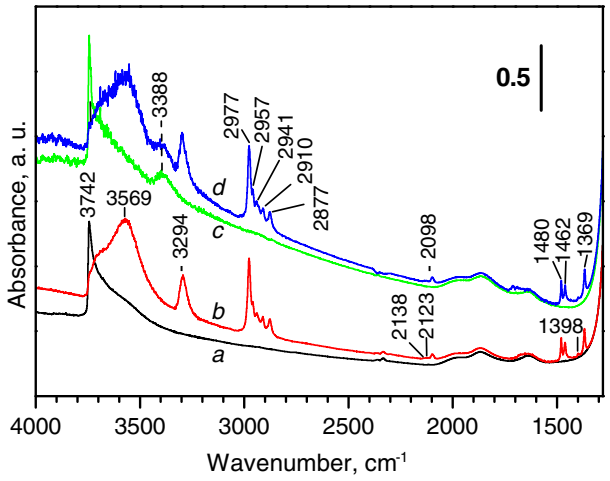

Fig. 8. IR spectrum of MCM-41-600N evacuated at 490 °C for 1 h (a) and after adsorption at r.t. of C_3H_4 (20 h Pa) (b). IR spectrum of MCM-41-900N evacuated at 490 °C for 1 h (c) and after adsorption at r.t. of C_3H_4 (20 h Pa) (d).

3.4. Basic properties detected by a base-catalyzed test reaction

The Knoevenagel condensation is a base-catalyzed reaction under mild conditions and is often used as a base-catalyzed test reaction to evaluate the basic properties of nitrogen-containing molecular sieves [18,21,27,30,33]. Here, the Knoevenagel condensation of benzaldehyde and malononitrile was used to probe the basic properties of the samples. All nitrided samples presented finite activity for the test reaction at 50 °C, and the selectivity to benzylidene malononitrile was close to 100%. In contrast, parent MCM-41 prior to nitridation showed negligible catalytic activity. These results indicate that basic sites can be formed on the surface of MCM-41 by nitridation. However, although the nitrogen content of the active catalysts is known to increase with the nitridation temperature (*vide supra*), this is not reflected in the conversion data (almost certainly because of the exceedingly high conversions in these preliminary measurements). It was suggested by Narasimharao et al. [30] that besides the nitrogen content, the nature of the framework nitrogen species also plays an important role in effecting the catalytic activity of benzaldehyde and high catalytic activity for Knoevenagel condensations may require both acidic (viz. Si–OH) and basic (viz. Si–NH_2) sites.

4. Conclusion

Mesoporous MCM-41 was prepared via a standard synthesis route and subsequently treated in flowing ammonia at elevated temperatures in the range between 600 and 950 °C. The goal was to prepare N-containing materials with basic properties which can be used as solid base catalysts. Physico-chemical properties were investigated by chemical analysis, N_2 adsorption, X-ray diffraction, ^{29}Si solid state NMR and IR spectroscopy. As already reported in the literature, the N content of the finished material could be controlled by the temperature during the nitridation procedure. The highest total N content was 26 wt.%. Transmission infrared spectroscopy suggested that the nitrogen is present in the samples as NH and NH_2 groups, and there was clear evidence for the location of the NH species in the bulk leading to the large width at half height of the N–H stretching band.

When the catalytic properties were tested in preliminary batch reactor experiments, the parent material MCM-41 was entirely inactive. In contrast, the N-containing materials showed finite activity for the Knoevenagel condensation reaction. This was the only indication for the presence of basic sites which provided some, though probably weak catalytic activity. This still qualitative experimental result was the only evidence for the presence of basic sites with no independent experimental proof being available.

For this reason we have attempted to collect additional information by recording the infrared spectra of acidic and basic probe molecules. Transmission infrared spectra of *in situ* pretreated sample wafers clearly showed that free unperturbed silanol groups were exposed on the surface.

The sole detectable NH vibration is the band at 3388 cm^{-1} which can be assigned to the N–H stretching mode of NH groups. This band is relatively broad. We therefore infer that these groups are not located at the surface but rather in the framework of the pore walls.

D_2 and D_2O exchange experiments (Fig. 5) show that the surface silanol groups undergo exchange of the protons with both molecules under relatively mild conditions, consistent with the inference that the groups are located on the surface. In contrast, D – exchange with NH groups required significantly more stringent temperature conditions.

The properties of the Si–OH were tested by CO adsorption. CO is a H-bond acceptor and hence provides information on the properties of the H-bond donors on the surface. The spectra show, that the Si–OH groups behave like very weakly acidic groups and very much resemble the properties of silanol groups on pure silica.

Chloroform $DCCl_3$ and methylacetylene CH_3CCH are CH-acids and form H-bonds with acceptor sites on the surface of basic materials. In the present case, these interactions could not be detected. The lack of H-bond interactions probably suggests that the basic sites on the surface of the nitrided MCM-41 are too weak or they are hidden or located in the framework, so that they are inaccessible. Chloroform and methylacetylene do not probe basic sites on the present nitrided MCM-41. However, they do form H-bonds with the silanols and function as H-bond acceptor via chlorine atoms or the triple bond, respectively.

Despite the spectroscopic evidence for the presence of silanol groups on the external pore walls, their formation mechanism still remains to be elucidated. Most likely the surface free energy of the hydroxylated surfaces is energetically more favorable than the nitrided surface.

In summary, the nitrogen in the present MCM-41 nitrogen-containing materials is present as NH and NH_2 species. The NH species are by far more abundant than the NH_2 species, and they are most likely located in the framework of the pore walls. These groups are not accessible for probe molecules and reactants. The NH_2 groups are minority species which might act as surface groups (e.g. basic sites) but which remain undetectable for probe molecules because of their extremely low density. We suggest that these amido groups are responsible for the basicity of the investigated nitrogen-containing MCM-41 materials. The base strength of these centers is likely sufficiently high to start the Knoevenagel condensation reaction, the overall activity of the catalyst, however, is low because of the low site density.

Acknowledgements

We gratefully acknowledge National Basic Research Program (also called 973 Program, nos. 2003CB615801 and 2009CB623502), National Natural Science Foundation (nos. 20573059 and 20777039) and International S&T Cooperation Program of China (no. 2007DFA90720).

References

[1] H. Hattori, Chem. Rev. 95 (1995) 537.
[2] T. Yashima, K. Sato, T. Hayasaka, N. Hara, J. Catal. 26 (1972) 303.
[3] A. Corma, S. Iborra, S. Miguel, Appl. Catal. 59 (1990) 237.
[4] A. Corma, S. Iborra, Adv. Catal. 49 (2006) 239.
[5] P.E. Hathaway, M.E. Davis, J. Catal. 116 (1989) 263.
[6] K.R. Kloetstra, H. van Bekkum, J. Chem. Soc., Chem. Commun. (1995) 1005.
[7] L.R.M. Martens, P.J. Grobet, P.A. Jacobs, Nature 315 (1985) 568.
[8] A. Corma, R.M. Martin-Aranda, F. Sanchez, J. Catal. 126 (1990) 192.
[9] M. Laspéras, T. Liorett, L. Chaves, I. Rodrigues, A. Chauvel, D. Brunel, Stud. Surf. Sci. Catal. 105 (1997) 75.
[10] R. Sercheli, A.L.B. Ferreira, M.C. Guerreiro, R.M. Vargas, R.A. Sheldon, U. Schuchardt, Tetrahedron Lett. 38 (1997) 1325.
[11] H. Yoshitake, T. Yokoi, T. Tatsumi, Chem. Mater. 14 (2002) 4603.
[12] J. Weitkamp, M. Hunger, U. Rymsa, Micropor. Mesopor. Mater. 48 (2001) 255.
[13] P. Llewellyn, S. Kaskel, in: F. Schüth, K.S.W. Sing, J. Weitkamp (Eds.), Handbook of Porous Solids, vol. 3, Wiley-VCH, Weinheim, 2002, p. 2078.
[14] L.M. Gandia, R. Malm, R. Marchand, R. Conanec, Y. Laurant, M. Mario, Appl. Catal. A: Gen. 114 (1994) L1.
[15] P. Grange, P. Bastians, R. Conanec, R. Marchand, Y. Laurant, Appl. Catal. A: Gen. 114 (1994) L191.
[16] M.J. Climent, A. Corma, V. Fornés, A. Frau, R. Guil-Lopez, S. Iborra, J. Primo, J. Catal. 163 (1996) 392.
[17] Y. Inaki, Y. Kajita, H. Yoshida, K. Ito, T. Hattori, J. Chem. Soc. Chem. Commun. (2001) 2358.
[18] Y. Xia, R. Mokaya, Angew. Chem. Int. Ed. 42 (2003) 2639.
[19] N. Chino, T. Okubo, Micropor. Mesopor. Mater. 81 (2005) 15.
[20] J. Wang, Q. Liu, Micropor. Mesopor. Mater. 83 (2005) 225.
[21] Y. Xia, R. Mokaya, J. Mater. Chem. 14 (2004) 2507.
[22] C. Zhang, Q. Liu, Z. Xu, J. Non-Cryst. Solids 351 (2005) 1377.
[23] J.C. Wang, Q. Liu, Chem. Commun. (2006) 900.
[24] K.S. Wan, Q. Liu, C.M. Zhang, Chem. Lett. 32 (2003) 362.
[25] K. Wan, Q. Liu, C.M. Zhang, J. Wang, Bull. Chem. Soc. Jpn. 77 (2004) 1409.
[26] G.T. Kerr, G.R. Shipman, J. Phys. Chem. 72 (1968) 3071.
[27] S. Ernst, M. Hartmann, S. Sauerbeck, T. Brongers, Appl. Catal. A: Gen. 200 (2000) 117.
[28] Y. Ono, T. Baba, Catal. Today 38 (1997) 321.
[29] J. Xiong, Y. Ding, H. Zhu, L. Yan, X. Liu, L. Lin, J. Phys. Chem. B 107 (2003) 1366.
[30] C. Zhang, Z. Xu, K. Wan, Q. Liu, Appl. Catal. A: Gen. 258 (2004) 55.
[31] X. Guan, N. Li, G. Wu, J. Chen, F. Zhang, N. Guan, J. Mol. Catal. A: Chem. 248 (2006) 220.
[32] X. Guan, F. Zhang, G. Wu, N. Guan, Mater. Lett. 60 (2006) 3141.
[33] K. Narasimharao, M. Hartmann, H.H. Thiel, S. Ernst, Micropor. Mesopor. Mater. 90 (2006) 377.
[34] L. Regli, S. Bordiga, C. Busco, C. Prestipino, P. Ugliengo, A. Zecchina, C. Lamberti, J. Am. Chem. Soc. 129 (2007) 12131.
[35] J.E. Haskouri, S. Cabrera, F. Sapina, J. Latorre, C. Guillem, A. Beltran-Porter, D. Beltran-Porter, M.D. Marcos, P. Amoros, Adv. Mater. 13 (2001) 192.
[36] L. Liu, G. Zhang, J. Dong, Acta Physico-Chim. Sin. 20 (2004) 65.
[37] M.A. Centeno, M. Debois, P. Grange, J. Phys. Chem. B 102 (1998) 6835.
[38] A. Corma, Chem. Rev. 97 (1997) 2373.
[39] J.Y. Ying, C.P. Mehnert, M.S. Wong, Angew. Chem. Int. Ed. 38 (1999) 56.
[40] R.V. Weeren, E.A. Leone, S. Curran, L.C. Klein, S.C. Danforth, J. Am. Ceram. Soc. 77 (1994) 2699.
[41] K. Nakamoto, Infrared Spectra of Inorganic and Coordination Compounds, Wiley, New York, 1962, p. 241.
[42] N. Fripiat, M.-A. Centeno, P. Grange, Chem. Mater. 11 (1999) 1434.
[43] G. Busca, V. Lorenzelli, G. Porcile, M.I. Baratron, P. Quintard, R. Marchand, Mater. Chem. Phys. 14 (1986) 123.
[44] J. Kaskel, K. Schlichte, J. Catal. 201 (2001) 370.
[45] E.A. Paukshtis, E.N. Yurchenko, Russ. Chem. Rev. 52 (1983) 42.
[46] M.C. Kung, H.H. Kung, Cat. Rev. – Sci. Eng. 27 (1985) 425.
[47] A.A. Davydov, Molecular Spectroscopy of Oxide Catalyst Surfaces, Wiley, New York, 2003.
[48] J.C. Lavalley, Trends Phys. Chem. 2 (1991) 305.
[49] J.C. Lavalley, Catal. Today 27 (1996) 377.
[50] J. Ryczkowski, Catal. Today 68 (2001) 263.
[51] H. Knözinger, S. Huber, J. Chem. Soc., Faraday Trans. 94 (1998) 2047.
[52] H. Knözinger, in: G. Ertl, H. Knözinger, F. Schüth, J. Weitkamp (Eds.), Handbook of Heterogeneous Catalysis, second ed., Wiley-VCH, Weinheim, 2008, p. 1135.
[53] M.I. Zaki, H. Knözinger, Mater. Chem. Phys. 17 (1987) 201.
[54] I. Mirsojew, S. Ernst, J. Weitkamp, H. Knözinger, Catal. Lett. 24 (1994) 235.
[55] E.A. Paukshtis, P.I. Soltanov, E.N. Yurchenko, K. Jiratova, Collect Czech. Chem. Commun. 47 (1982) 2044.
[56] S. Huber, H. Knözinger, J. Mol. Catal. A: Chem. 141 (1999) 117.
[57] D. Mordenti, P. Grotz, H. Knözinger, Catal. Today 70 (2001) 83.
[58] T.P. Beebe, P. Gelin, J.T. Yates Jr., Surf. Sci. 148 (1984) 526.
[59] G. Ghiotti, E. Garrone, C. Morterra, F. Boccuzzi, J. Phys. Chem. 83 (1979) 2863.
[60] H. Knözinger, in: P. Schuster, G. Zundel, C. Sandorfy (Eds.), The Hydrogen Bond, vol. 3, North-Holland, Amsterdam, New York, Oxford, 1976, p. 1265.
[61] K. Hadjiivanov, A. Penkova, M.A. Centeno, Catal. Commun. 8 (2007) 1715.